Hindawi Publishing Corporation
Advances in High Energy Physics
Volume 2016, Article ID 5308084, 10 pages
http://dx.doi.org/10.1155/2016/5308084

Research Article

A Universal Description of Pseudorapidity Distributions in Both Nucleus-Nucleus and p-p Collisions at Currently Available Energies

Z. J. Jiang, H. P. Deng, and Y. Huang

College of Science, University of Shanghai for Science and Technology, Shanghai 200093, China

Correspondence should be addressed to Z. J. Jiang; jzj265@163.com

Received 27 January 2016; Revised 17 April 2016; Accepted 5 May 2016

Academic Editor: Victor Roy

Investigations have shown that the collective motion appears not only in nucleus-nucleus but also in p-p collisions. The best tool for depicting such collective motion is relativistic hydrodynamics. In this paper, the collective motion is assumed to obey the hydrodynamic model which integrates the features of Landau and Hwa-Bjorken theory and is one of a very few analytically solvable models. The fluid is then supposed to freeze out into charged particles from a space-like hypersurface with a fixed time of t_{FO}. The investigations of present paper show that this part of charged particles together with leading particles, which, by conventional definition, carry on the quantum numbers of colliding nucleons and take away the most part of incident energy, can give a proper universal description to the pseudorapidity distributions of charged particles measured in both nucleus-nucleus and p-p collisions at currently available energies.

1. Introduction

In recent years, especially with the operations of BNL-RHIC and after CERN-LHC, the nature of matter created in nucleus or particle collisions has been undergoing extensive and deep experimental and theoretical investigations. One of the most important achievements arrived at from these investigations is that the matter formed in collisions shows the characteristics of collective motion as a nearly perfect fluid with a small shear viscosity over entropy density [1–31].

The best approach to describing the spatiotemporal evolution of the fluid-like matter is the relativistic hydrodynamics, which was first put forward by Landau in his pioneering work in 1953 [32]. Owing to the high degree of nonlinearity and interconnection of hydrodynamic equations, numerical simulations are, as usual, widely employed to deal with them especially for 2- or 3-dimensional expansions or situations including viscosity. In numerical simulations, besides a powerful calculation system, there is also a need of a sophisticated skill for avoiding instabilities in solving partial differential hydrodynamic equations.

From the time of Landau till now, the analytical solutions of hydrodynamics are mainly limited to 1 + 1 expansions for a perfect fluid with a simple equation of state [8–17]. There are also a few analytical discussions about 2 + 1 or 3 + 1 flows [18, 19]. Along with the discovery of collective motion of matter created in high energy physics in recent years, the analytical work has entered into a stage of rapid developments and achieved a number of good results. For example, by generalizing the relation between ordinary rapidity and space-time rapidity, [9] integrates Landau and Hwa-Bjorken [33, 34] two models together, proposing a model called unified hydrodynamics in this paper and presenting a set of exact solutions. By taking advantage of the traditional scheme of Khalatnikov potential [35], [10] solved analytically the hydrodynamic equations and gave a pack of simple exact solutions for a perfect fluid with a linear equation of state. By taking into account the work done by the fluid elements on each other, [11–13] generalized the Hwa-Bjorken model for an accelerationless system to the model for an accelerated one and obtained a class of exact analytical solutions of relativistic hydrodynamics.

One of the most important applications of 1 + 1 dimensional hydrodynamics is the analysis of the pseudorapidity distributions of charged particles in high energy physics. In the present paper, combing the effects of leading particles, we will discuss such kinds of distributions in the framework of unified hydrodynamics for both nucleus-nucleus and p-p collisions at currently available energies. In this theoretical model, the produced charged particles are divided into two parts. One is from the freeze-out of the fluid which is located in the central rapidity region. The other is from leading particles which are situated in the projectile or target fragmentation region with Gauss rapidity distributions normalized to the number of participants. Hence, the established model involves the charged particles produced in the whole rapidity region.

The paper is organized as follows. First, in Section 2, we give a brief introduction to the theoretical model, presenting the exact solutions of unified hydrodynamic model and giving the rapidity distributions of charged particles resulted from both fluid and leading particles. The model is then made a comparison in Section 3 between experimental observations performed by PHOBOS Collaboration at BNL-RHIC in Au-Au collisions at $\sqrt{s_{\mathrm{NN}}} = 200\,\mathrm{GeV}$ [36] and by ALICE Collaboration at CERN-LHC in Pb-Pb collisions at $\sqrt{s_{\mathrm{NN}}} = 2.76\,\mathrm{TeV}$ [37]. In Section 4, the theoretical model continues to undergo a test in p-p collisions at energies from 23.6 to 7000 GeV [38–41]. The last section is traditionally about conclusions.

2. A Brief Description of the Model

The key ingredients of the model are as follows.

(1) The evolution of the fluid-like matter created in collisions is dominated by the energy-momentum conservation:

$$\frac{\partial T^{\mu\nu}}{\partial x^{\nu}} = 0, \quad \mu, \nu = 0, 1, \tag{1}$$

where $x^{\nu} = (x^0, x^1) = (t, z)$, t is the time and z is the longitudinal component of coordinates along beam direction. $T^{\mu\nu}$ is the energy-momentum tensor, which, for a perfect fluid, takes the form as

$$T^{\mu\nu} = (\varepsilon + p)\, u^{\mu} u^{\nu} - p g^{\mu\nu}, \tag{2}$$

where $g^{\mu\nu} = g_{\mu\nu} = \mathrm{diag}(1, -1)$, u^{μ}, ε, and p are the metric tensor, 4-velocity, energy density, and pressure of the fluid, respectively. For a constant speed of sound, ε and p are related by the equation of state:

$$\varepsilon = g p, \tag{3}$$

where $1/\sqrt{g} = c_{\mathrm{s}}$ is the speed of sound. Equations (2) and (3) make (1) translate to

$$\begin{aligned} g\partial_{+} \ln p &= -\frac{(g+1)^2}{2}\partial_{+} y - \frac{g^2-1}{2} e^{-2y} \partial_{-} y, \\ g\partial_{-} \ln p &= \frac{(g+1)^2}{2}\partial_{-} y + \frac{g^2-1}{2} e^{2y} \partial_{+} y, \end{aligned} \tag{4}$$

where ∂_{+} and ∂_{-} are the compact notation of partial derivatives with respect to light-cone coordinates $z_{\pm} = t \pm z = x_0 \pm x_1 = \tau e^{\pm \eta_{\mathrm{S}}}$, $\tau = \sqrt{z_{+} z_{-}}$ is the proper time, $\eta_{\mathrm{S}} = 1/2 \ln(z_{+}/z_{-})$ is the space-time rapidity, and y is the ordinary rapidity of the fluid.

(2) Equation (4) is a set of complicated differential equations with high nonlinearity and coupling between variables p and y. In order to solve it, the relation between y and η_{S} is generalized to the form [9]:

$$2y = \ln u_{+} - \ln u_{-} = \ln F_{+}(z_{+}) - \ln F_{-}(z_{-}), \tag{5}$$

where $u_{\pm} = u_0 \pm u_1 = e^{\pm y}$ are the light-cone components of 4-volicity, and $F_{\pm}(z_{\pm})$ are the two arbitrary functions. In case of

$$F_{\pm}(z_{\pm}) = z_{\pm}, \tag{6}$$

(5) reduces to $y = \eta_{\mathrm{S}}$, returning to the boost-invariant picture of Hwa-Bjorken. Otherwise, (5) describes the non-boost-invariant geometry of Landau. Accordingly, (5) unifies the Landau with Hwa-Bjorken hydrodynamics. It plays a role of bridge between these two models.

By using (5), (4) becomes

$$\begin{aligned} g\partial_{+} \ln p &= -\frac{(g+1)^2}{4}\frac{f_{+}'}{f_{+}} + \frac{g^2-1}{4}\frac{f_{-}'}{f_{+}}, \\ g\partial_{-} \ln p &= -\frac{(g+1)^2}{4}\frac{f_{-}'}{f_{-}} + \frac{g^2-1}{4}\frac{f_{+}'}{f_{-}}, \end{aligned} \tag{7}$$

where the prime stands for the derivatives with respect to z_{+} or z_{-}, $f_{\pm} = F_{\pm}/H$, and H is an arbitrary constant. Completing the integration of the above equation, it becomes

$$\begin{aligned} g \ln p &= -\frac{(g+1)^2}{4} \ln f_{+} + \frac{g^2-1}{2}\sqrt{\ln f_{+} \ln f_{-}} \\ &\quad + \Delta_{-}(z_{-}), \\ g \ln p &= -\frac{(g+1)^2}{4} \ln f_{-} + \frac{g^2-1}{2}\sqrt{\ln f_{+} \ln f_{-}} \\ &\quad + \Delta_{+}(z_{+}). \end{aligned} \tag{8}$$

In order to keep the consistency of the above two equations, $\Delta_{\pm}(z_{\pm})$ should take

$$\Delta_{\pm}(z_{\pm}) = -\frac{(g+1)^2}{4} \ln(f_{\pm}). \tag{9}$$

Inserting them into (8), we can obtain the final solution [9]:

$$\begin{aligned} s(z_{+}, z_{-}) &= s_0 \left(\frac{p}{p_0}\right)^{g/(g+1)} \\ &= s_0 \exp\left[-\frac{g+1}{4}\left(l_{+}^2 + l_{-}^2\right) + \frac{g-1}{2} l_{+} l_{-}\right], \end{aligned} \tag{10}$$

where s is the entropy density of the fluid and s_0 is its initial scale. g, as mentioned above, takes as a constant in this paper, and

$$l_{\pm}(z_{\pm}) = \sqrt{\ln f_{\pm}},$$
$$y(z_+, z_-) = \frac{1}{2}\left(l_+^2 - l_-^2\right), \tag{11}$$
$$z_{\pm} = 2h\int_0^{l_{\pm}} e^{u^2}\,\mathrm{d}u,$$

$h = H/A$, and A is an arbitrary constant fitting condition:

$$F_{\pm}F_{\pm}'' = \frac{A^2}{2}, \tag{12}$$

where the double prime represents the second derivatives with respect to z_+ or z_-. As $A = 0$, the above equation reduces to $F_{\pm}'' = 0$ which gives the solution of $F_{\pm}(z_{\pm}) = z_{\pm} + c$, returning to the Hwa-Bjorken case of (6) up to a constant c. Hence, the values of A or $h = H/A$ describe the deviation of system from Hwa-Bjorken expansions.

(3) As the expansion of the fluid lasts to the time of t_{FO}, the inelastic interactions between the particles in the fluid cease, and the ratios of different kinds of particles remain unchanged. At this moment, the collective motion of the fluid comes to an end, and the fluid decouples or freezes out into the detected particles from a space-like hypersurface with a fixed time of t_{FO}. The rapidity distributions of entropy of the fluid at this hypersurface take the form:

$$\frac{\mathrm{d}S}{\mathrm{d}y} = su^{\mu}\frac{\mathrm{d}\lambda_{\mu}}{\mathrm{d}y}\bigg|_{t_{\mathrm{FO}}} = su^{\mu}n_{\mu}\frac{\mathrm{d}\lambda}{\mathrm{d}y}\bigg|_{t_{\mathrm{FO}}}, \tag{13}$$

where n^{μ} is the 4-dimensional unit vector normal to the hypersurface:

$$n^{\mu}n_{\mu} = n_+n_- = 1. \tag{14}$$

$\mathrm{d}\lambda^{\mu} = \mathrm{d}\lambda n^{\mu}$, and $\mathrm{d}\lambda$ is the space-like infinitesimal length element along hypersurface:

$$\mathrm{d}\lambda = \sqrt{\mathrm{d}\lambda^{\mu}\mathrm{d}\lambda_{\mu}} = \sqrt{-\mathrm{d}z^+\mathrm{d}z^-}, \tag{15}$$

where the minus sign accounts for the space-like characteristic of $\mathrm{d}\lambda$. Considering that the number of charged particles is proportional to the amount of entropy; from solution (10) and (13), we can obtain the rapidity distributions of the produced charged particles [9]:

$$\frac{\mathrm{d}N_{\mathrm{Fluid}}}{\mathrm{d}y} = Ce^{-(g-1)(l_+-l_-)^2/4}\left.\frac{\partial_+\phi e^{y} + \partial_-\phi e^{-y}}{\partial_+\phi l_- e^{y} + \partial_-\phi l_+ e^{-y}}\right|_{t_{\mathrm{FO}}}, \tag{16}$$

where C is an overall normalization constant. ϕ stands for an arbitrary space-like hypersurface.

(4) The right-hand side of (16) is evaluated on the space-like hypersurface with the time equaling t_{FO}. Such hypersurface can be therefore taken as

$$\phi(z_+, z_-) = t_{\mathrm{FO}} = \frac{1}{2}(z_+ + z_-) = C, \tag{17}$$

where C is an arbitrary constant. This equation gives

$$\partial_{\pm}\phi = \frac{1}{2}. \tag{18}$$

Thus, (16) turns into

$$\frac{\mathrm{d}N_{\mathrm{Fluid}}}{\mathrm{d}y} = C\frac{e^{-(g-1)(l_+-l_-)^2/4}}{l_- + l_+ + (l_- - l_+)\tanh y}. \tag{19}$$

(5) In nucleus or particle collisions, apart from the freeze-out of the fluid, leading particles also have certain contribution to the measured charged particles. Leading particles are believed to be formed outside the nucleus, that is, outside the colliding region [42, 43]. The motion and generation of leading particles are therefore free from hydrodynamic descriptions. As we have argued before that the rapidity distribution of leading particles takes the Gaussian form [15, 16],

$$\frac{\mathrm{d}N_{\mathrm{Lead}}}{\mathrm{d}y} = \frac{N_{\mathrm{Lead}}}{\sqrt{2\pi}\sigma}\exp\left\{-\frac{\left[|y| - y_0\right]^2}{2\sigma^2}\right\}, \tag{20}$$

where N_{Lead}, y_0, and σ are the number of leading particles, central position, and width of distribution, respectively. This conclusion comes from the consideration that, for a given incident energy, different leading particles resulting from each time of collisions have approximately the same amount of energy or rapidity. Then, the central limit theorem [44, 45] guarantees the plausibility of the above argument. Actually, experimental measurements have shown that any kind of charged particles presents a good Gaussian rapidity distribution [46–48].

y_0 in (20) is the average position of leading particles. It should increase with incident energies and centrality cuts. The value of σ relies on the relative energy or rapidity differences among leading particles. It should not, at least not apparently, depend on the incident energies, centrality cuts, and even colliding systems. The specific values of y_0 and σ can be determined by tuning the theoretical predictions to experimental data.

By definition, leading particles mean the particles inheriting the quantum numbers of colliding nucleons. Hence, the number of leading particles is equal to that of participants. For p-p collisions, there are only two leading particles. They are separately in the projectile and target fragmentation region. For an identical nucleus-nucleus collision, the number of leading particles

$$N_{\mathrm{Lead}} = \frac{N_{\mathrm{Part}}}{2}, \tag{21}$$

where N_{Part} is the total number of participants, which can be determined in theory by Glauber model [49, 50].

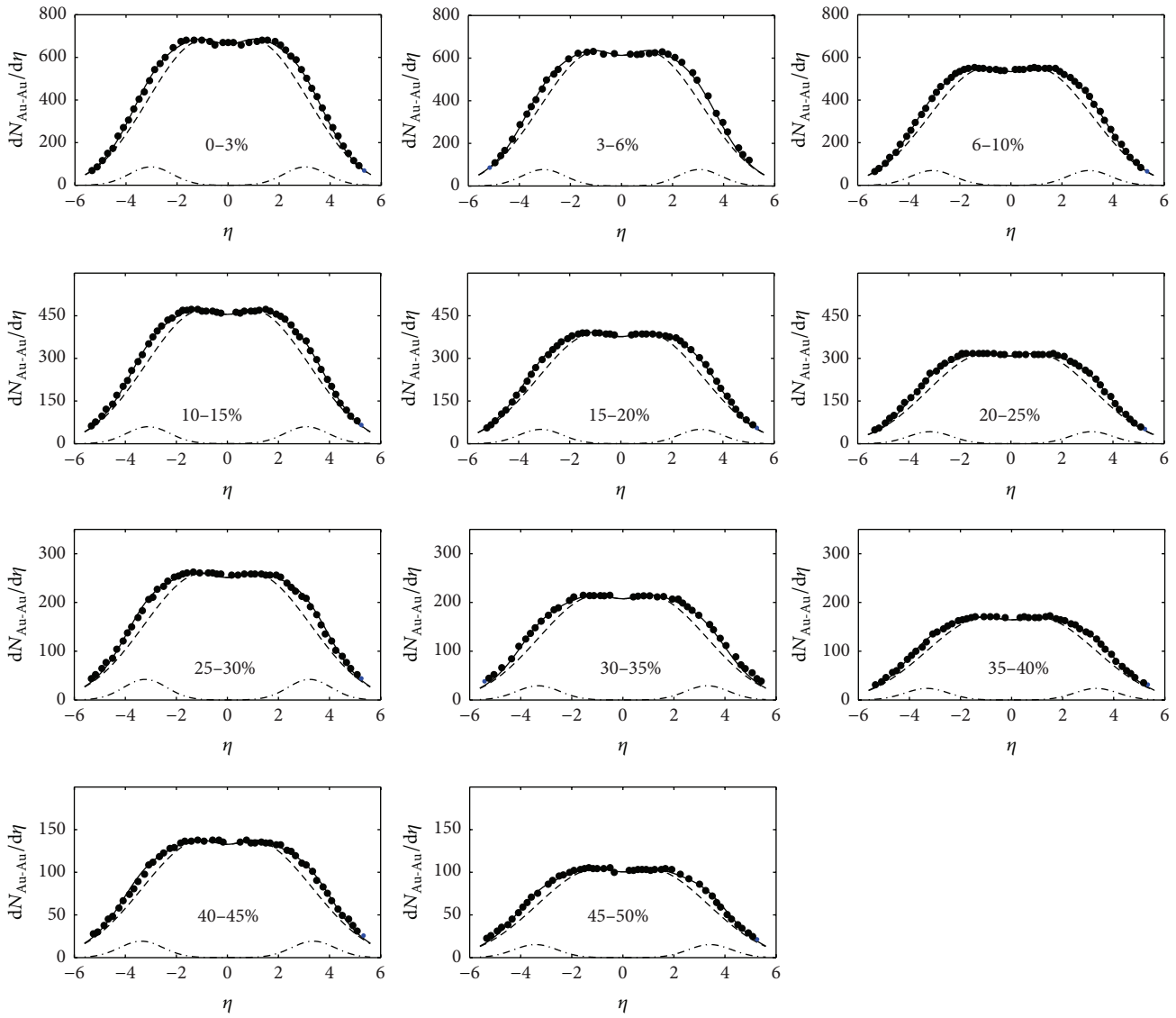

FIGURE 1: The pseudorapidity distributions of produced charged particles in different centrality Au-Au collisions at $\sqrt{s_{NN}} = 200$ GeV. The solid dots are the experimental measurements [36]. The dashed curves are the results from unified hydrodynamics of (19). The dashed-dotted curves are the results from leading particles of (20). The solid curves are the sums of dashed and dashed-dotted curves.

3. Comparison with Experimental Measurements in Nucleus-Nucleus Collisions

Having rapidity distributions of (19) and (20), the pseudorapidity distribution measured in experiments can be expressed as

$$\frac{dN}{d\eta} = \sqrt{1 - \frac{m^2}{m_T^2 \cosh^2 y}}\,\frac{dN}{dy}, \tag{22}$$

$$y = \frac{1}{2}\ln\left[\frac{\sqrt{p_T^2\cosh^2\eta + m^2} + p_T \sinh\eta}{\sqrt{p_T^2\cosh^2\eta + m^2} - p_T \sinh\eta}\right], \tag{23}$$

where p_T is the transverse momentum, $m_T = \sqrt{m^2 + p_T^2}$ is the transverse mass, and

$$\frac{dN}{dy} = \frac{dN_{Fluid}}{dy} + \frac{dN_{Lead}}{dy} \tag{24}$$

is the total rapidity distribution from both the freeze-out of the fluid and leading particles.

Substituting (24) or (19) and (20) into (22), we can get the pseudorapidity distributions of the charged particles. The results are shown in Figures 1 and 2, which are for different centrality Au-Au and Pb-Pb collisions at $\sqrt{s_{NN}} = 200$ GeV and 2.76 TeV, respectively. The solid dots in the figures are the experimental measurements [36, 37]. The dashed curves are the results got from unified hydrodynamics of (19). The dashed-dotted curves are the results obtained from leading

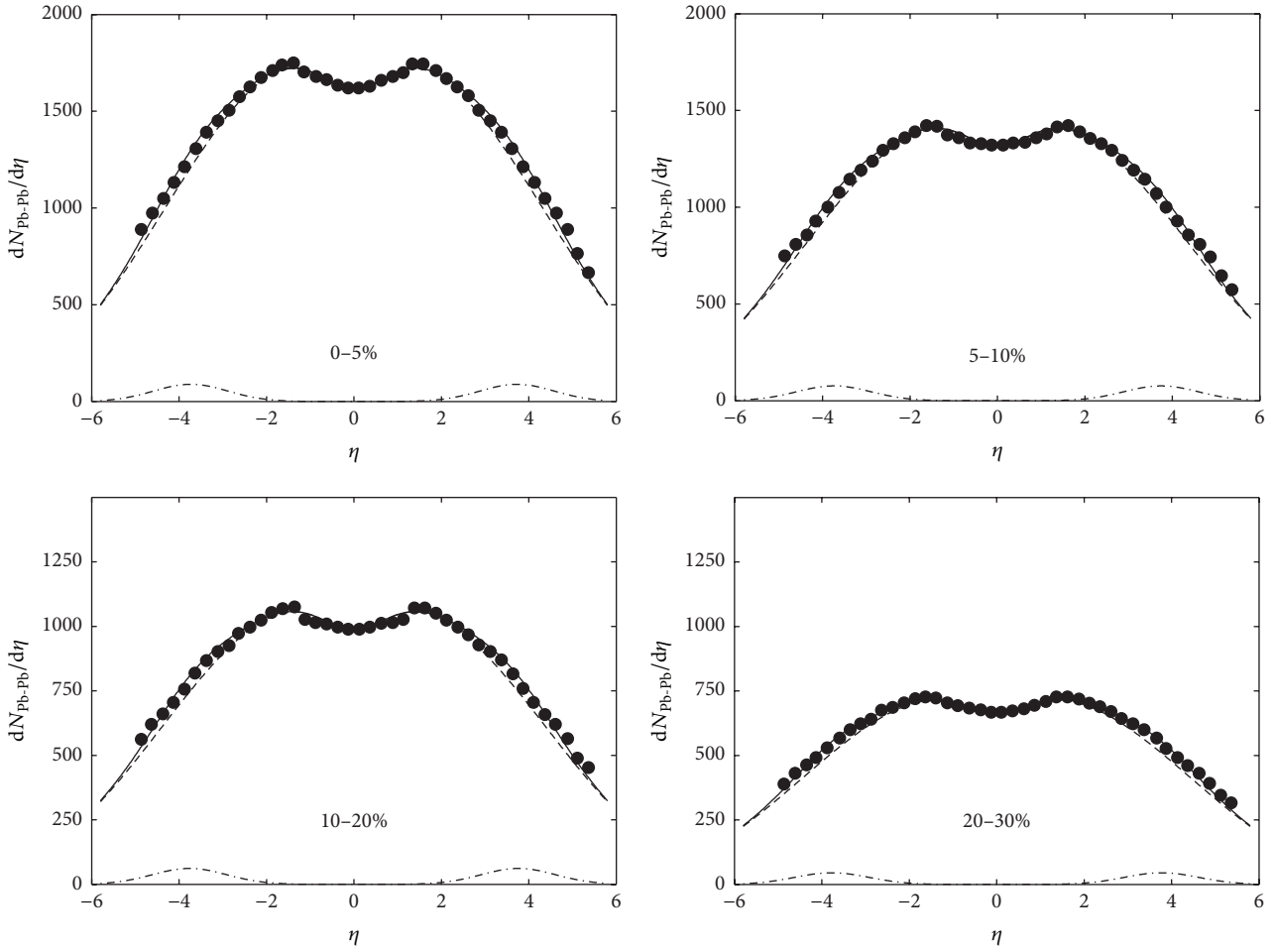

FIGURE 2: The pseudorapidity distributions of produced charged particles in different centrality Pb-Pb collisions at $\sqrt{s_{NN}} = 2.76$ TeV. The solid dots are the experimental measurements [37]. The dashed curves are the results from unified hydrodynamics of (19). The dashed-dotted curves are the results from leading particles of (20). The solid curves are the sums of dashed and dashed-dotted curves.

particles of (20). The solid curves are the sums of dashed and dashed-dotted curves. It can be seen that the combined contributions from both unified hydrodynamics and leading particles match up well with experimental data.

Experiments have shown that the overwhelming majority of charged particles produced in heavy ion collisions at high energy consists of pions, kaons, and protons with proportions of about 83%, 12%, and 5%, respectively [51]. These proportions are not evidently dependent on colliding energies and systems. Furthermore, for a given incident energy, the transverse momentum p_T changes very slowly with centrality cut. For a specific type of charged particle, it can be well taken to be a constant for centrality cuts from 0–55%, which we are interested in. In Au-Au collisions at $\sqrt{s_{NN}} = 200$ GeV, this constant is about 0.45, 0.65, and 0.93 GeV/c for pions, kaons, and protons, respectively. In calculations, the mass and transverse momentum in (22) and (23) take the values of $m = 0.22$ GeV and $p_T = 0.50$ GeV/c in Au-Au collisions at $\sqrt{s_{NN}} = 200$ GeV, which are the mean values of those of pions, kaons, and protons. In Pb-Pb collisions at $\sqrt{s_{NN}} = 2.76$ TeV, they take the values of $m = 0.22$ GeV and $p_T = 0.62$ GeV/c. Here, p_T takes the mean value from experimental measurements [4].

The factor g in (3) takes the values of 6.6 and 4.5, respectively, for different centrality Au-Au and Pb-Pb collisions. That is, it decreases with increasing energies. It should change like this. Since g decreases with increasing temperature of the fluid [52], and the higher the energy, the higher the temperature of the created fluid.

The normalization constant C in (19) takes the values of $(6.45, 6.07, 5.31, 4.56, 3.84, 3.12, 2.57, 2.15, 1.71, 1.39, 1.06) \times 10^3$ and $(1.74, 1.44, 1.08, 0.74) \times 10^4$ for centrality cuts from smaller to larger in Au-Au and Pb-Pb collisions, respectively. The parameter h in (11) takes the values of $(5.41, 3.08, 2.53, 2.05, 1.01, 0.92, 0.83, 0.55, 0.47, 0.36, 0.22) \times 10^{-4}$ and $(1.02, 0.78, 0.51, 0.29) \times 10^{-5}$ for centrality cuts from smaller to larger in Au-Au and Pb-Pb collisions, respectively. It can be seen that h decreases with increasing energies and centrality cuts. It should vary in this way. Since the larger the energy and centrality cut, the more transparent the nucleus. The produced charged particles will then be located in a wider rapidity region. While, the region of rapidity distributions

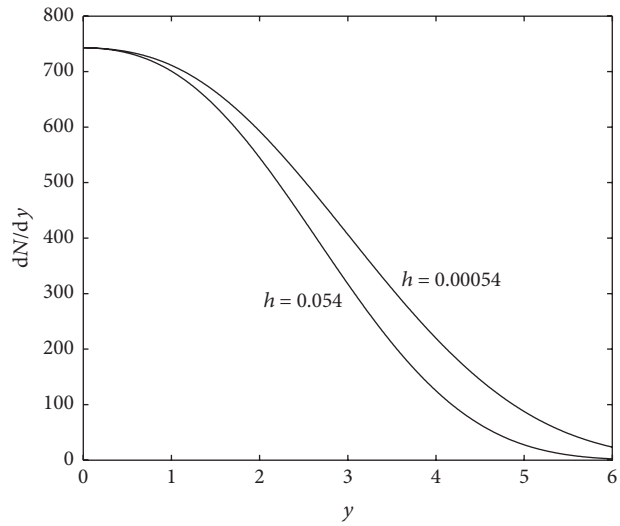

Figure 3: The rapidity distributions of produced charged particles for two different h values in Au-Au collisions normalized to 0–3% centrality cut.

of (19) is mainly determined by h. The wider the region of rapidity distributions, the smaller the value of h. This can be seen in Figure 3, which is for Au-Au collisions normalized to 0–3% centrality cut. The wider curve is the corresponding rapidity distribution in Figure 1, obtained by using $h = 5.41 \times 10^{-4}$. The narrower one is for $h = 5.41 \times 10^{-2}$. Hence, the region of rapidity distributions decreases with increasing h. This forms the basis for the above fitted h values.

The central parameter y_0 in (20) takes the values of 2.91, 2.93, 2.95, 2.98, 3.01, 3.05, 3.10, 3.17, 3.20, 3.25, and 3.30 and 3.61, 3.62, 3.64, and 3.65 for centrality cuts from smaller to larger in Au-Au and Pb-Pb collisions, respectively. As mentioned above, it increases with centrality cuts and energies. The width parameter σ in (20) takes a constant of $\sigma = 0.85$ for different centrality cuts in both Au-Au and Pb-Pb collisions. As stated above, it is irrelevant to centrality cuts, incident energies, and colliding systems.

4. Comparison with Experimental Measurements in p-p Collisions

Compared with nucleus-nucleus collisions, p-p collisions are a relatively simpler and smaller system and therefore produce the matter in a much tinier volume. If such matter expands in the same way as that generated in nucleus-nucleus collisions has been experiencing endless disputations.

Such situation has changed since a series of findings in recent years [20–31]. The investigations of [20] have shown that the hydrodynamic predictions of multiplicity productions in p-p ($\overline{\text{p}}$) or e^+-e^- collisions at even several of GeV match up well with experimental data. The measurements from CMS Collaboration at CERN-LHC have shown that [21], just like in nucleus-nucleus collisions, the ridge structures, the signal of collective motion, also appear in p-p collisions. References [22, 23] further substantiated that these observed ridge structures can be well understood in the framework of hydrodynamics. In [24], the STAR Collaboration at BNL-RHIC has measured the HBT (Hanbury-Brown-Twiss) radii for p-p collisions as a function of multiplicity. The measured results are well favored by the predictions of hydrodynamic models made in [25–27].

In [28, 29], Sarkisyan et al. utilized the combined model of Landau hydrodynamics plus combinations of the constituent quarks in participants to deal with the multihadron productions and transverse momentum distributions in p-p ($\overline{\text{p}}$) collisions. By employing the hydrodynamic solutions known as Gubser flow [18], [30] demonstrated the collective radial flow of high multiplicity p-p collisions. In our previous work [31], we used the evolution-dominated hydrodynamics together with the effects of leading particles to describe the pseudorapidity distributions of charged particles produced in p-p collisions. At present paper, from (19) and (20), we can also get such distributions. The results are shown in Figure 4 for p-p collisions at energies from 23.6 to 900 GeV. The solid dots are the experimental measurements [38–40]. The dashed curves are the results from unified hydrodynamics of (19). The dashed-dotted curves are the results from leading particles of (20). The solid curves are the sums of dashed and dashed-dotted curves. It can be seen that the theoretical results are in well consistent with experimental data.

In calculations, as in Au-Au or Pb-Pb collisions, the mass m in (22) and (23) takes the value of 0.22 GeV. The transverse momentum p_{T} varies with energies according to relation [41]:

$$p_{\text{T}} = 0.413 - 0.0171 \ln(s) + 0.00143 \ln^2(s), \quad (25)$$

where p_{T} and $\sqrt{s}$ are in units of GeV/c and GeV, respectively. The width parameter σ in (20) takes the same value as that in nucleus-nucleus collisions; that is, $\sigma = 0.85$. This certifies the above argument again that σ is independent of energies and colliding objects. The factors g, h, and y_0 take the values of 8.4–5.2, 18.4–4.0 $\times 10^{-5}$, and 1.91–3.00, respectively, for energies from lower to higher. Just as in nucleus-nucleus collisions, g and h decrease with increasing energies, and,

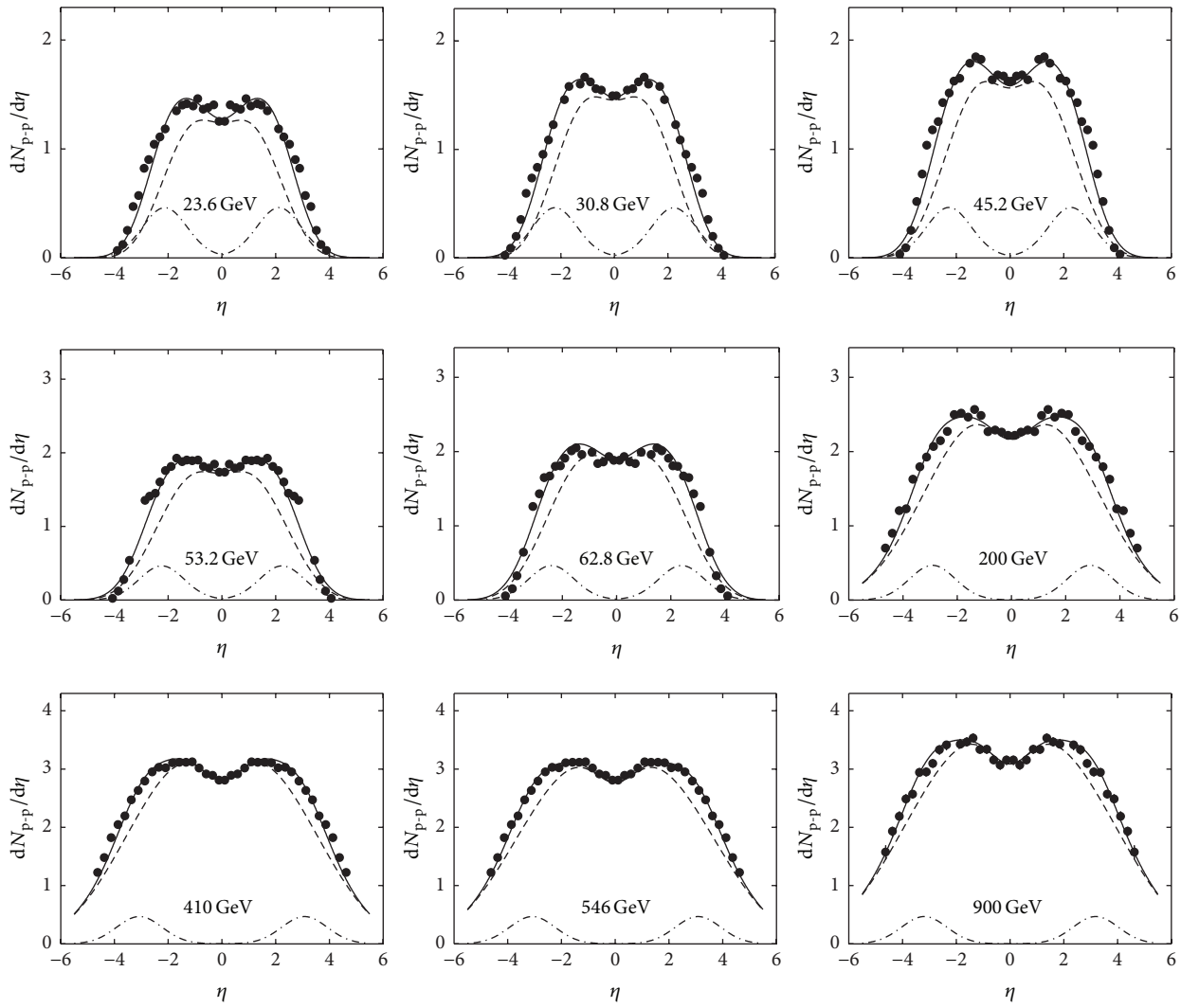

FIGURE 4: The pseudorapidity distributions of produced charged particles in p-p collisions at energies from $\sqrt{s} = 23.6$ to 900 GeV. The solid dots are the experimental measurements [38–40]. The dashed curves are the results from unified hydrodynamics of (19). The dashed-dotted curves are the results from leading particles of (20). The solid curves are the sums of dashed and dashed-dotted curves.

y_0, on the contrary, increases with energies. Their variations against energies are presented in Figure 5. The solid dots represent the above fitted values. The solid curves are drawn from relations

$$g = 11.3311 - 0.5324 \ln s + 0.0065 \ln^2 s,$$
$$\ln h = 23.3049 - 3.7056 \ln s + 0.0877 \ln^2 s, \quad (26)$$
$$y_0 = 0.3657 + 0.2709 \ln s - 0.0055 \ln^2 s,$$

where $\sqrt{s}$ is in units of GeV. It can be seen that all the solid dots are well seated on the curves. The stars and circles in this figure are the corresponding predictions for p-p collisions at CERN-LHC energies of 2.36 and 7 TeV, respectively. From these predictions, we can get the pseudorapidity distributions of produced charged particles in these two situations, and the results are shown in Figure 6. The solid dots are the experimental data [41]. The dashed curves are the predicted results from unified hydrodynamics of (19). The dashed-dotted curves are the predicted results from leading particles of (20). The solid curves are the sums of dashed and dashed-dotted curves. It can be seen that the theoretical predictions agree well with the available measurements in the midpseudorapidity regions.

At the end of this section, we would like to point out that, at present, we have no knowledge about the viscosities in matter created in TeV energies especially for small system of p-p collisions. Here, just as what we have done in case of nucleus-nucleus collisions at RHIC energies, we ignore the viscous effects for the purpose of simplifications.

5. Conclusions

The charged particles in nucleus and particle collisions are supposed to have the same producing mechanism. That is,

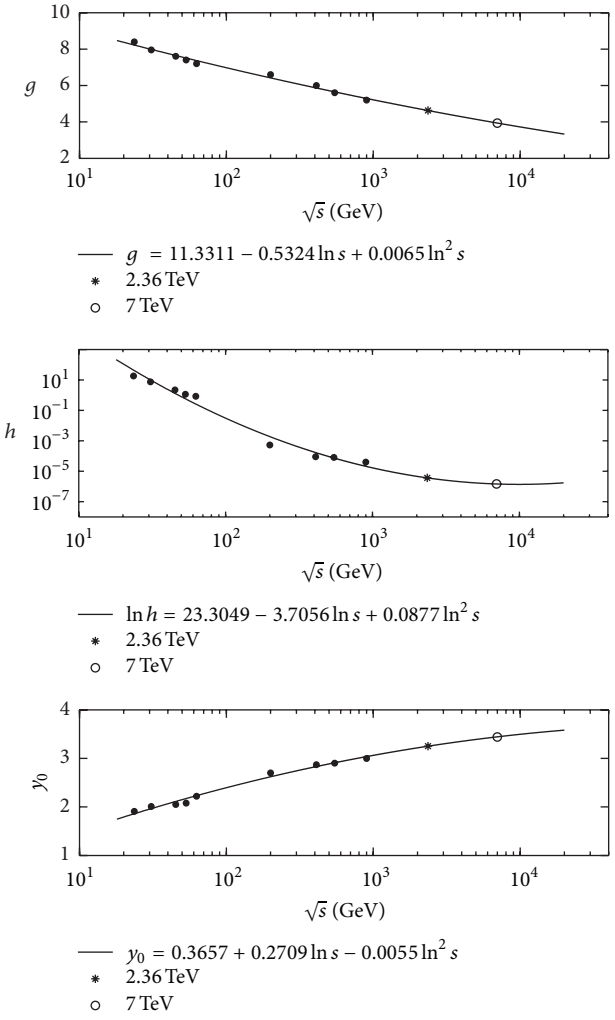

FIGURE 5: The variations of g, h, and y_0 against $\sqrt{s}$. The solid dots represent the fitted values given in the text. The stars and circles are the predictions for p-p collisions at CERN-LHC energies of $\sqrt{s} = 2.36$ and 7 TeV, respectively.

one part is from the freeze-out of the fluid-like matter, and the other is from leading particles.

The fluid-like matter is assumed to evolve according to the relativistic hydrodynamics, which incorporates the characteristics of Landau and Hwa-Bjorken hydrodynamic model *via* a generalizing relation between ordinary rapidity y and space-time rapidity η_S. This is one of a very few hydrodynamic models which can be solved analytically. The solutions can then be utilized to formulate the rapidity distributions of charged particles frozen out from a space-like hypersurface with a fixed time of t_{FO}. In the derived formula, there are two parameters g and h. Known from comparing with experimental measurements, both g and h decrease with increasing energies, and, in nucleus-nucleus collisions, g maintains unchanged for different centrality cuts, while h decreases with increasing centrality cut.

For leading particles, their rapidity distributions are, as usual, believed possessing the Gaussian form normalized to a constant equaling the number of participants, which can be figured out in theory. This assumption is based on the consideration that, for a given incident energy, the leading particles have about the same energy, and coincides with the fact that any kind of the charged particles produced in collisions takes on well the Gaussian form of rapidity distribution. It is interesting to note that the width of Gaussian rapidity distribution σ is irrelevant to the energies, centrality cuts, and colliding systems.

Comparing with experimental measurements, we can see that the pseudorapidity distributions of the produced charged particles in both nucleus-nucleus and p-p collisions at currently available energies can be well described in a universal manner of unified hydrodynamics plus leading particles.

Competing Interests

The authors declare that there are no competing interests regarding the publication of this paper.

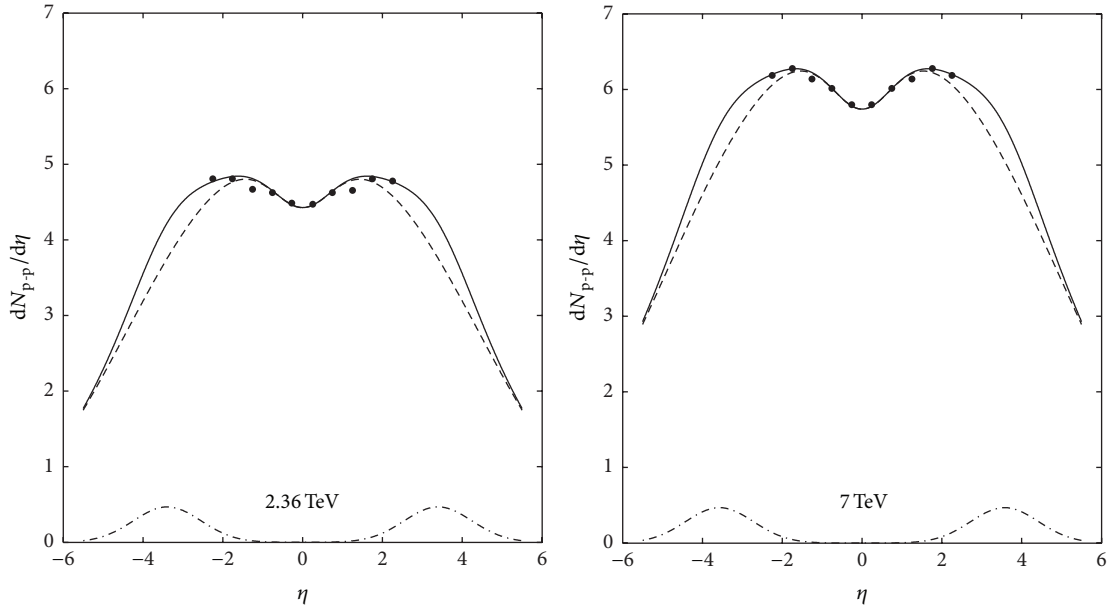

FIGURE 6: The pseudorapidity distributions of produced charged particles in p-p collisions at energies of $\sqrt{s}$ = 2.36 and 7 TeV. The solid dots are the experimental measurements [41]. The dashed curves are the predicted results from unified hydrodynamics of (19). The dashed-dotted curves are the predicted results from leading particles of (20). The solid curves are the sums of dashed and dashed-dotted curves.

Acknowledgments

This work is partly supported by the Hujiang Foundation of China with Grant no. B14004 and Shanghai Key Lab of Modern Optical System.

References

[1] S. S. Adler, S. Afanasiev, C. Aidala et al., "Elliptic flow of identified Hadrons in Au + Au collisions at $\sqrt{s_{NN}}$ = 200 GeV," *Physical Review Letters*, vol. 91, Article ID 182301, 2003.

[2] J. Adams, C. Adler, M. M. Aggarwal et al., "Azimuthal anisotropy at the relativistic heavy ion collider: the first and fourth harmonics," *Physical Review Letters*, vol. 92, no. 6, Article ID 062301, 6 pages, 2004.

[3] K. Aamodt, B. Abelev, A. Abrahantes Quintana et al., "Higher harmonic anisotropic flow measurements of charged particles in Pb-Pb collisions at $\sqrt{s_{NN}}$ = 2.76 TeV," *Physical Review Letters*, vol. 107, Article ID 032301, 2011.

[4] S. Chatrchyan, V. Khachatryan, A. M. Sirunyan et al., "Measurement of the elliptic anisotropy of charged particles produced in PbPb collisions at $\sqrt{s_{NN}}$ = 2.76 TeV," *Physical Review C*, vol. 87, no. 1, Article ID 014902, 34 pages, 2013.

[5] G. Aad, B. Abbott, J. Abdallah et al., "Measurement of the pseudorapidity and transverse momentum dependence of the elliptic flow of charged particles in lead–lead collisions at $\sqrt{S_{NN}}$ = 2.76TeV with the ATLAS detector," *Physics Letters B*, vol. 707, no. 3-4, pp. 330–348, 2012.

[6] C. Gale, S. Jeon, and B. Schenke, "Hydrodynamic modeling of heavy-ion collisions," *International Journal of Modern Physics A*, vol. 28, no. 11, Article ID 1340011, 2013.

[7] U. Heinz and R. Snellings, "Collective flow and viscosity in relativistic heavy-ion collisions," *Annual Review of Nuclear and Particle Science*, vol. 63, pp. 123–151, 2013.

[8] A. Bialas and R. Peschanski, "Asymmetric (1+1)-dimensional hydrodynamics in high-energy collisions," *Physical Review C*, vol. 83, no. 5, Article ID 054905, 2011.

[9] A. Bialas, R. A. Janik, and R. Peschanski, "Unified description of Bjorken and Landau 1+1 hydrodynamics," *Physical Review C*, vol. 76, no. 5, Article ID 054901, 2007.

[10] G. Beuf, R. Peschanski, and E. N. Saridakis, "Entropy flow of a perfect fluid in (1+1) hydrodynamics," *Physical Review C - Nuclear Physics*, vol. 78, no. 6, Article ID 064909, 2008.

[11] T. Csörgő, M. I. Nagy, and M. Csanád, "New family of simple solutions of relativistic perfect fluid hydrodynamics," *Physics Letters B*, vol. 663, no. 4, pp. 306–311, 2008.

[12] M. I. Nagy, T. Csörgő, and M. Csanád, "Detailed description of accelerating, simple solutions of relativistic perfect fluid hydrodynamics," *Physical Review C*, vol. 77, no. 2, Article ID 024908, 2008.

[13] M. Csanád, M. I. Nagy, and S. Lökös, "Exact solutions of relativistic perfect fluid hydrodynamics for a QCD Equation of State," *European Physical Journal A*, vol. 48, article 173, 2012.

[14] C. Y. Wong, "Landau hydrodynamics reexamined," *Physical Review C*, vol. 78, no. 5, Article ID 054902, 2008.

[15] Z. J. Jiang, Q. G. Li, and H. L. Zhang, "Revised Landau hydrodynamic model and the pseudorapidity distributions of charged particles produced in nucleus-nucleus collisions at maximum energy at the BNL Relativistic Heavy Ion Collider," *Physical Review C*, vol. 87, no. 4, Article ID 044902, 2013.

[16] Z. J. Jiang, Y. Zhang, H. L. Zhang, and H. P. Deng, "A description of the pseudorapidity distributions in heavy ion collisions at RHIC and LHC energies," *Nuclear Physics A*, vol. 941, pp. 188–200, 2015.

[17] M. S. Borshch and V. I. Zhdanov, "Exact solutions of the equations of relativistic hydrodynamics representing potential flows," *Symmetry, Integrability and Geometry: Methods and Applications (SIGMA)*, vol. 3, article 116, 11 pages, 2007.

[18] S. S. Gubser, "Symmetry constraints on generalizations of Bjorken flow," *Physical Review D*, vol. 82, no. 8, Article ID 085027, 2010.

[19] Y. Hatta, B. W. Xiao, and D. L. Yang, "Non-boost-invariant solution of relativistic hydrodynamics in 1 + 3 dimensions," *Physical Review D*, vol. 93, no. 1, Article ID 016012, 2016.

[20] P. Steinberg, "Landau hydrodynamics and RHIC phenomena," *Acta Physica Hungarica*, vol. 24, no. 1, pp. 51–57, 2005.

[21] V. Khachatryan, A. M. Sirunyan, A. Tumasyan et al., "Observation of long-range near-side angular correlations in proton-proton collisions at the LHC," *Journal of High Energy Physics*, vol. 2010, article 91, 2010.

[22] K. Werner, I. Karpenko, and T. Pierog, "'Ridge' in proton-proton scattering at 7 TeV," *Physical Review Letters*, vol. 106, no. 12, Article ID 122004, 4 pages, 2011.

[23] P. Bożek, "Elliptic flow in proton–proton collisions at $\sqrt{s}$ = 7 TeV," *The European Physical Journal C*, vol. 71, article 1530, 2011.

[24] M. Aggarwal, Z. Ahammed, A. V. Alakhverdyants et al., "Pion femtoscopy in $p+p$ collisions at $\sqrt{s}$ = 200 GeV," *Physical Review C*, vol. 83, no. 6, Article ID 064905, 2011.

[25] V. M. Shapoval, P. Braun-Munzinger, Iu. A. Karpenko, and Yu. M. Sinyukov, "Femtoscopic scales in p+p and p+Pb collisions in view of the uncertainty principle," *Physics Letters B*, vol. 725, no. 1–3, pp. 139–147, 2013.

[26] Y. M. Sinyukov and V. M. Shapoval, "Correlation femtoscopy of small systems," *Physical Review D*, vol. 87, no. 9, Article ID 094024, 2013.

[27] Y. Hirono and E. Shuryak, "Femtoscopic signature of strong radial flow in high-multiplicity *pp* collisions," *Physical Review C*, vol. 91, no. 5, Article ID 054915, 2015.

[28] E. K. G. Sarkisyan and A. S. Sakharov, "Relating multihadron production in hadronic and nuclear collisions," *European Physical Journal C*, vol. 70, no. 3, pp. 533–541, 2010.

[29] A. N. Mishra, R. Sahoo, E. K. G. Sarkisyan, and A. S. Sakharov, "Effective-energy budget in multiparticle production in nuclear collisions," *European Physical Journal C*, vol. 74, article 3147, 2014.

[30] T. Kalaydzhyan and E. Shuryak, "Collective flow in high-multiplicity proton-proton collisions," *Physical Review C*, vol. 91, no. 5, Article ID 054913, 2015.

[31] Z. Jiang, H. Zhang, K. Ma, and J. Wang, "A description of pseudorapidity distributions in p-p collisions at center-of-mass energy from 23.6 to 900 GeV," *Chinese Physics C*, vol. 39, no. 4, Article ID 044102, 2015.

[32] L. D. Landau, "On the multiple production of particles in fast particle collisions," *Izvestiya Akademii Nauk SSSR. Seriya Matematicheskaya*, vol. 17, p. 51, 1953 (Russian).

[33] R. C. Hwa, "Statistical description of hadron constituents as a basis for the fluid model of high-energy collisions," *Physical Review D*, vol. 10, no. 7, pp. 2260–2268, 1974.

[34] J. D. Bjorken, "Highly relativistic nucleus-nucleus collisions: the central rapidity region," *Physical Review D*, vol. 27, no. 1, pp. 140–151, 1983.

[35] I. M. Khalatnikov, "Some questions of the relativistic hydrodynamics," *Journal of Experimental and Theoretical Physics*, vol. 27, pp. 529–541, 1954 (Russian).

[36] B. Alver, B. B. Back, M. D. Baker et al., "Charged-particle multiplicity and pseudorapidity distributions measured with the PHOBOS detector in Au + Au, Cu + Cu, d + Au, and p + p collisions at ultrarelativistic energies," *Physical Review C*, vol. 83, no. 2, Article ID 024913, 2011.

[37] E. Abbas, B. Abelev, J. Adam et al., "Centrality dependence of the pseudorapidity density distribution for charged particles in Pb-Pb collisions at $\sqrt{s_{NN}}$ = 2.76 Tev," *Physics Letters B*, vol. 726, no. 4-5, pp. 610–622, 2013.

[38] W. Thomé, K. Eggert, K. Giboni et al., "Charged particle multiplicity distributions in pp collisions at ISR energies," *Nuclear Physics B*, vol. 129, no. 3, pp. 365–389, 1977.

[39] G. J. Alner, R. E. Ansorge, B. Åsman et al., "Scaling of pseudorapidity distributions at c.m. energies up to 0.9 TeV," *Zeitschrift für Physik C: Particles and Fields*, vol. 33, no. 1, pp. 1–6, 1986.

[40] B. Alver, B. B. Back, M. D. Baker et al., "Charged-particle multiplicity and pseudorapidity distributions measured with the PHOBOS detector in Au + Au, Cu + Cu, d + Au, and p + p collisions at ultrarelativistic energies," *Physical Review C*, vol. 83, Article ID 024913, 2011.

[41] V. Khachatryan, A. M. Sirunyan, A. Tumasyan et al., "Transverse-momentum and pseudorapidity distributions of charged hadrons in *pp* Collisions at $\sqrt{s}$ = 7TeV," *Physical Review Letters*, vol. 105, no. 2, Article ID 022002, 2010.

[42] A. Berera, M. Strikman, W. S. Toothacker, W. D. Walker, and J. J. Whitmore, "The limiting curve of leading particles from hadron-nucleus collisions at infinite A," *Physics Letters, Section B: Nuclear, Elementary Particle and High-Energy Physics*, vol. 403, no. 1-2, pp. 1–7, 1997.

[43] J. J. Ryan, *Proceeding of Annual Meeting of the Division of Particles and Fields of the APS*, World Scientific, Singapore, 1993.

[44] T. B. Li, *The Mathematical Processing of Experiments*, Science Press, Beijing, China, 1980 (Chinese).

[45] J. Voit, *The Statistical Mechanics of Financial Markets*, Springer, Berlin, Germany, 3rd edition, 2005.

[46] M. Murray and F. T. Collaboration, "Scanning the phases of QCD with BRAHMS," *Journal of Physics G: Nuclear and Particle Physics*, vol. 30, no. 8, pp. S667–S674, 2004.

[47] M. Murray, "Flavor dynamics," *Journal of Physics G: Nuclear and Particle Physics*, vol. 35, no. 4, Article ID 044015, 2008.

[48] I. G. Bearden, D. Beavis, C. Besliu et al., "Charged meson rapidity distributions in central Au + Au collisions at $\sqrt{s_{NN}}$ = 200TeV," *Physical Review Letters*, vol. 94, no. 16, Article ID 162301, 2005.

[49] Z. J. Jiang, Y. F. Sun, and Q. G. Li, "The energy and centrality dependences of the pseudorapidity distributions of the charged particles in Au+Au collisions," *International Journal of Modern Physics E*, vol. 21, no. 1, Article ID 1250002, 2012.

[50] Z.-J. Jiang, "The numbers of participants and nucleon-nucleon collisions in high-energy heavy-ion collisions," *Acta Physica Sinica*, vol. 56, no. 9, pp. 5191–5195, 2007 (Chinese).

[51] S. S. Adler, S. Afanasiev, C. Aidala et al., "Identified charged particle spectra and yields in Au + Au collisions at $\sqrt{s_{NN}}$ = 200 Gev," *Physical Review C*, vol. 69, no. 3, Article ID 034909, 32 pages, 2004.

[52] A. Adare, S. Afanasiev, C. Aidala et al., "Scaling properties of azimuthal anisotropy in Au + Au and Cu + Cu collisions at $\sqrt{s_{NN}}$ = 200TeV," *Physical Review Letters*, vol. 98, no. 16, Article ID 162301, 2007.